ELSEVIER

Physica C 329 (2000) 45–50

PHYSICA C

www.elsevier.nl/locate/physc

Fluctuation-enhanced conductivity in $YBa_2Cu_3O_x$ $(6.5 \leq x \leq 6.95)$ and $Tl_2Ba_2Ca_2Cu_3O_{10\pm\delta}$ superconducting thin films

J.Y. Juang *, M.C. Hsieh, C.W. Luo, T.M. Uen, K.H. Wu, Y.S. Gou

Department of Electrophysics, National Chiao-Tung University, 30047 Hsin-chu, Taiwan

Received 14 September 1999; accepted 20 October 1999

Abstract

The fluctuation-induced conductivity $(\Delta\sigma(T))$ near T_c of a sole $YBa_2Cu_3O_x$ (YBCO) film with various precisely controlled oxygen contents $(6.5 \leq x \leq 6.95)$ was studied and compared with those obtained from its Tl-based counterparts. For YBCO films with $x > 6.7$, $\Delta\sigma(T)$ displays a distinct 3D to 2D crossover as the temperature approaches T_c. On the other hand, as $T \to T_c$, $\Delta\sigma(T)$ of both Tl-based and YBCO film with $x \leq 6.7$ exhibits a reversed 2D to 3D crossover. It is suggestive that the coupling between the CuO_2 layers may have changed significantly with reducing oxygen. © 2000 Elsevier Science B.V. All rights reserved.

Keywords: Fluctuation effects; Oxygen stoichiometry; Cu-chains; Coherence length

1. Introduction

Since the discovery of the high-temperature superconductors (HTS), the dimensionality of the materials has been one of the most pursued issues as it lays the ground for constructing the high-T_c superconductivity. Questions such as whether substantial coupling between slabs of CuO_2 planes is a necessity for high-T_c superconductivity have received much attention. Early studies [1–3] of fluctuation-enhanced conductivity on optimum-doped YBCO thin films and single crystals have reached the conclusions that the material is quasi-two-dimensional (Q2D) in nature with very short zero-temperature c-axis coherence length $\xi_c(0)$ $(0.45 \sim 1.8$ Å) and a rather scattered values of effective fluctuation thickness d_{eff} $(1.7 \sim 11.7$ Å). Subsequent extensive studies [4] indicated that for fully oxygenated YBCO, the physically reasonable parameters should be $\xi_c(0)$ ~ 1.5 Å and $d_{\text{eff}} \sim 11.8$ Å, respectively. Despite the above consensus, however, the issue of dimensional crossover has remained as a matter of debate [5]. On the other hand, alternative approach of using artificial HTS superlattices with various thicknesses and materials of superconducting and non-superconducting ''spacers'' has been tried, as well [6]. From these studies, it appeared that long-range Josephson coupling does occur and is important in superlattices with metallic spacers. Unfortunately, most of the ''peculiar properties'' obtained in these artificial sys-

* Corresponding author. Tel.: +886-3-571-2121; fax: +886-3-572-5230.

E-mail address: jyjuang@cc.nctu.edu.tw (J.Y. Juang)

PII: S0921-4534(99)00566-3

tems seemed to stem mainly from extrinsic factors, thus, may not reflect the intrinsic properties of HTS.

A direct evidence indicating that HTS compounds are native superconducting superlattices themselves was the observation of intrinsic Josephson effects exhibited in $Bi_2Sr_2CaCu_2O_8$ (Bi-2212) single crystals by Kleiner et al. [7]. The evidence guarantees the essential validity of the model of Josephson-coupled Q2D superconducting slabs (with a junction thickness of approximately 15 Å) in describing the HTS. However, as noted by Kleiner and Müller [8], the fully oxygenated YBCO was an exception in their observations. This implies that either YBCO is not Josephson-coupled (e.g., the material may form S–S′–S structure) or the effects may be obscured by defects. In order to explore these issues, a direct monitoring of the junction structure without encountering the complications arising from the detailed microstructure and defect of the films should be of interest. In this study, a single YBCO film was used to investigate the $\Delta\sigma(T)$ behavior as a function of film oxygen content. It was observed that both d_{eff} and $\xi_c(0)$ decreased drastically with reducing film oxygen content. These changes are translated into the coupling strength between the CuO_2 slabs. The results are compared with that obtained from the more two-dimensional single grain Tl-2223 films.

2. Experiment

The YBCO films used in this study were deposited by a KrF excimer pulsed laser on $LaAlO_3(100)$ substrates at 760°C with an oxygen pressure of 0.28 Torr. The energy density and the repetition rate of the laser pulse were 2–4 J/cm^2 and 3–10 Hz, respectively. The as-deposited films typically have zero-resistance temperature of 89–90 K with *c*-axis oriented normal to the substrate surface. The oxygen content of the YBCO film was manipulated by an encapsulated bulk annealing method [9]. As will be discussed in detail below, this method is capable of controlling the oxygen content of the YBCO films precisely and reversibly. It is noted that by using this method, all the measurements can be performed on a single film. As a result, any changes in the superconducting properties should arise mainly from the effects of the oxygen content and possible complications originated from individual film structures are minimized. On the other hand, for the Tl-2223 samples studied, the measuring bridges were formed entirely on a single grain [10]. All the transport measurements were carried out by the standard four-probe technique.

3. Results and discussion

Fig. 1 shows the typical in-plane resistivity as a function of temperature $\rho_{ab}(T)$ for YBCO films with various oxygen contents. It is noted that at fully oxygenated state, $\rho_{ab}(T)$ is described neatly by the linear expression $\rho_{ab}(T) = \rho_{ab}(0) + \alpha T$ with $\rho_{ab}(0)$ and α being -11 μΩ cm and 1.5 μΩ cm/K, respectively. These extrapolated values agree extremely well with those obtained for YBCO single crystals [3], indicating that the quality of the present films should be viable for revealing the intrinsic properties of the material. Furthermore, as displayed in the inset of Fig. 1, the T_{c0} decreases from 90.3 K of the fully oxygenated state through the distinct two-plateau feature of YBCO system [11] with descending oxygen content. This is indicative that the oxygen content of the films was indeed varied as expected.

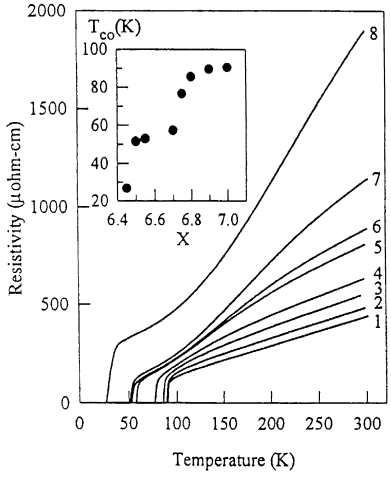

Fig. 1. $\rho_{ab}(T)$ for a YBCO film with various oxygen contents. Curves 1 to 8 represent $x = 7.0$, 6.9, 6.8, 6.75, 6.7, 6.55, 6.5, and 6.45, respectively. The inset shows the T_{c0} as a function of x.

To demonstrate the ''reversibility'' and the ''immunity'' (i.e., properties other than those directly associate with oxygen content were not affected) of the present oxygen controlling technique, repeated annealing at several conditions was carried out. As can be seen in Fig. 2, results for $x = 7.0$, $x = 6.8$, $x = 6.7$, and $x = 6.5$ indeed demonstrate the viability of the process in manipulating the oxygen content in YBCO films. We note that although slightly deviations in details are observable, the important features of the whole $\rho_{ab}(T)$ are evidently reproduced. Considering the sensitivity of the transport properties to the film oxygen content (see below) and the inevitable fluctuations of the annealing facility, the present results are truly remarkable. First of all, it indicates that only the oxygen content was varied. If there were any accompanied variations in microstructure or crystalline defects during each annealing scheme, a much more complicated $\rho_{ab}(T)$ variation is expected. More importantly, it implies that the specific features of $\rho_{ab}(T)$ are truly intrinsic and are intimately associated with the state at each oxygen content. The question now is how to encompass all the drastic changes in $\rho_{ab}(T)$ into a simple picture of reducing oxygen. Clearly, by simply attributing it to hole concentration changes [11] would not be adequate.

The linear $\rho_{ab}(T)$ observed with $x \geq 0.8$ ($T_{c0} \approx 85$–90 K) has been interpreted to arise from some kind of inelastic scattering [5,12]. On the other hand, a downturn (S shape) in $\rho_{ab}(T)$ is clearly observed when the film is significantly underdoped ($x \leq 6.7$). This downturn is now generally believed to arise from the opening of the spin gap below T^* which leads to the freezing off of spin fluctuation scattering [13]. Optical and resistivity data indicate the development of a pseudogap below T^* for the transport in the *c*-direction [13,14]. As will be seen below, this also reflects when the Cu–O chain mediated coupling unique to the YBCO system is completely suppressed. Apparently, in the $x \leq 6.7$ regime there is no direct way of deriving $\Delta\sigma(T)$ from $\rho_{ab}(T)$ because of the intervening of the pseudogap effects. Consequently, in the remaining of this study, we will concentrate on analyzing fluctuation effects at states where $\rho_{ab}(T)$ remains linear. Incidentally, it was found that $x \approx 6.7$ not only represents the beginning of the $T_{c0} = 60$ K plateau but also depicts a dimensional crossover state of the YBCO system.

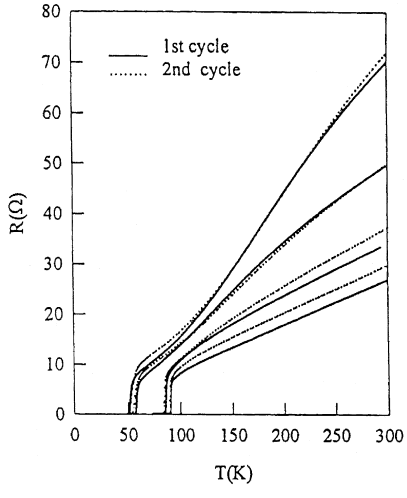

Fig. 2. $R(T)$ curves for $x = 7.0$, 6.8, 6.7, and 6.5 for the first (solid curves) and the second (dotted curves) annealing cycle.

As pointed out by Landau and Lifshitz [15], for the effects of thermal fluctuations to become significant and observable experimentally, the required condition is $k_B T \gg \hbar/\tau$. Here τ is a time characterizing the rate of change for some physical quantity to return to its equilibrium state. For a system describable by the linearized time-dependent Ginzburg–Landau (TDGL) theory, the thermal fluctuations are expected to become significant only when $k_B T \gg \hbar/\tau_{GL}$. With $\tau_{GL} = \pi\hbar/8k_B(T - T_c)$ [16], one expects to observe fluctuation-enhanced conductivity only when $T < 1.65T_c$. In this study, only the data between T_c and $T \ll 1.65T_c$ will be used for analyzing $\Delta\sigma(T)$. We define $\Delta\sigma(T) = 1/\rho_m(T) - 1/\rho_l(T)$ with ρ_m(T) and $\rho_l(T)$ being the measured and linearly extrapolated (from room temperature) in-plane resistivities, respectively.

According to Aslamazov and Larkin (AL) [17], $\Delta\sigma(T)$ can have distinct functional forms depending on the dimensionality of the system, which in turn is a strong function of the temperature range under discussion. Namely, when $d_{eff} \ll \xi(T)$ and the system is considered as 2D, $\Delta\sigma(T)$ becomes

$$\Delta\sigma(T) = \left(e^2/16\hbar d_{eff}\right)\varepsilon^{-1}, \quad (1)$$

where $\varepsilon \equiv (T - T_c)/T_c$ is the reduced temperature and the critical temperature T_c is inferred from the

maximum of $d\rho(T)/dT$. Whereas, when $d_{\text{eff}} \gg \xi(T)$ and the system becomes 3D,

$$\Delta\sigma(T) = \left[e^2/32\hbar\xi_c(0)\right]\varepsilon^{-1/2}. \quad (2)$$

Eqs. (1) and (2) can be rewritten as:

$$1/\left[\Delta\sigma^2(T)\varepsilon\right] = \left(16\hbar d_{\text{eff}}/e^2\right)^2\varepsilon \quad (3)$$

and

$$1/\left[\Delta\sigma^2(T)\varepsilon\right] = \left(32\hbar\xi_c(0)/e^2\right)^2 \quad (4)$$

for 2D and 3D cases, respectively. The apparent linear ε-dependence and ε-independent form of $1/[\Delta\sigma^2(T)\varepsilon]$ in each case should allow one to locate the temperature range reflecting the dimensionality of the system easily. Thus, one can use the appropriate functional form to derive the corresponding physical parameters of the specific state. We note that this is different from the methods used by previous researchers where the dimensional crossover region usually was not well-defined [1–4].

Indeed, as shown in Fig. 3, the plots of $1/[\Delta\sigma^2(T)\varepsilon]$ vs. ε for $x > 6.8$ conditions evidently display distinct regions characterizing the corresponding dimensionalities. Three regions are immediately identified. Starting from higher temperatures, a nonlinear region (I), an essentially constant region (II), and a linear region (III) are observed with decreasing temperatures. In region I, since $\rho_{ab}(T)$ is no longer describable by the A–L scenario

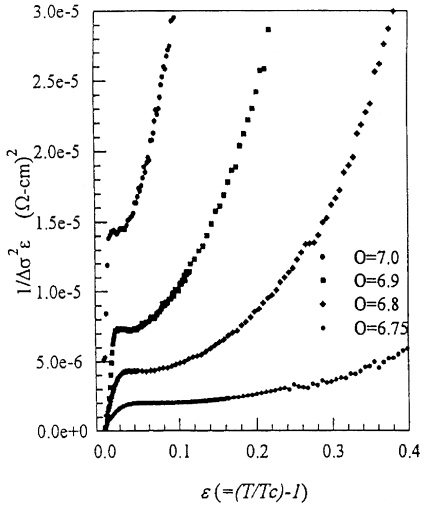

Fig. 3. $1/[\Delta\sigma^2(T)\varepsilon]$ as function of ε for YBCO with $x > 6.7$. Notice the curves display clear dimensional crossover.

Table 1
Physical parameters obtained from $\Delta\sigma(T)$ analyses discussed in the text

	$x \approx 7.0$	$x \approx 6.9$	$x \approx 6.8$	$x \approx 6.75$	$x \approx 6.7$	Tl-2223
T_c (K)	90.6	89.6	85.9	77.2	57.9	108.4
T_{cr} (K)	91.6	90.9	88.3	80.3	–	109.2
$\xi_c(0)$ (Å)	2.9	2.0	1.6	1.0	0.6	0.2
d_{eff} (Å)	60.3	39.9	21.3	11.8	–	4.4
$\xi_c(T_{cr})$ (Å)	27.6	16.6	9.6	5.0	–	1.9
$d_{\text{eff}}/2\xi_c(T_{cr})$	1.1	1.2	1.1	1.2	–	1.2

because of the diminishing fluctuation-induced effects due to $\tau_{GL} < \tau_{e-p} \approx 0.4$ ps (τ_{e-p} is the relaxation time of electron–phonon interaction) [18], we will not analyze it further. Nonetheless, if we take region II and III as manifestation of thermal fluctuation-enhanced conductivity and analyze the data within the framework of A–L theory (i.e., Eq. (3) and (4)), systematic variations of d_{eff} and $\xi_c(0)$ with the oxygen content of the YBCO film are revealed. The results are summarized in Table 1.

The fact that $\xi_c(0)$ of the fully oxygenated state (≈ 2.9 Å) agrees well with that obtained by the upper critical field measurements [1] indicates the viability of the present analyses. Nonetheless, there are several features which needed some further discussion. First of all, we note that the ''width'' of the dimensional characteristic temperature range and the crossover temperature T_{cr} changed systematically with the oxygen content. The widening of region III (i.e., $T_c - T_{cr}$) with the decreasing oxygen content clearly indicates a more 2D characteristic of the system. Second, although within the first T_c-plateau ($6.8 < x < 7.0$) the T_{c0} values decreased only slightly, both $\xi_c(0)$ and d_{eff} dropped drastically with decreasing x. To further elucidate this peculiar trend, we define a parameter $\xi_c(T_{cr})$ by using $\xi_c(T) \equiv \xi_c(0) \times \epsilon^{1/2}$ to determine when the system will always exhibit 2D behavior [16] and plot $\xi_c(0)$, d_{eff}, and $\xi_c(T_{cr})$ as a function of x in Fig. 4. It is interesting to observe that they are all extrapolated to intercept at $x \approx 6.7$. The results are discussed below by encompassing the recent microscopic structural changes associated with oxygen depletion in YBCO system.

Right from the beginning of the HTS studies, it is known that the Cu–O chain is the most prominent sector to be affected by removing oxygen from the

YBCO system [11]. The long-range order structure characterized by a metallic conduction behavior is interrupted by the depletion of the oxygen at the chain site, leading to short-range oxygen ordering structure [19]. Such microscopic rearrangements of the O(1) (chain site) oxygen have been found to give rise the non-metallic conduction and tremendous structural diffuse scattering [19–21]. The consensus reached in these studies is that the retention of the long-range order Cu–O chain is the most prominent factor of obtaining enough hole doping in the CuO_2 planes and the coupling strength between them. The hole density accounts for high-T_c. Whereas the degree of the Cu–O chain ordering affects $\xi_c(0)$ and hence, the coupling interaction necessitated for the effective conducting thickness extending over several unit cells along the *c*-axis. Within this scenario, the dimensional crossover from 3D to 2D is determined primarily by the divergence of $\xi_c(T)$ near T_c, as was observed here.

The above argument further implies that when $x \leq 6.7$, the Cu–O chain mediated coupling unique to the YBCO system is completely suppressed. Thus, the system is expected to behave more like the non-chained Bi-based and Tl-based HTS. This is indeed observed by comparing the results obtained from a single grain Tl-2223 system. As is evident from Fig. 5, $\Delta\sigma(T)$ of both Tl-2223 and $x = 6.7$ YBCO clearly displays a 2D to 3D crossover with

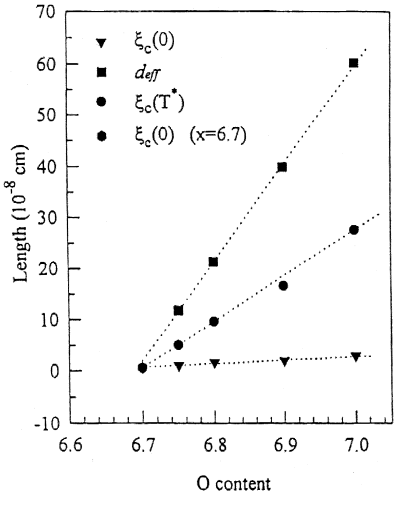

Fig. 4. Plots of d_{eff}, $\xi_c(0)$, and $\xi_c(T_{\text{cr}})$ as a function of x. Notice the dotted lines (to guide the eye) intersect at $x \sim 6.7$.

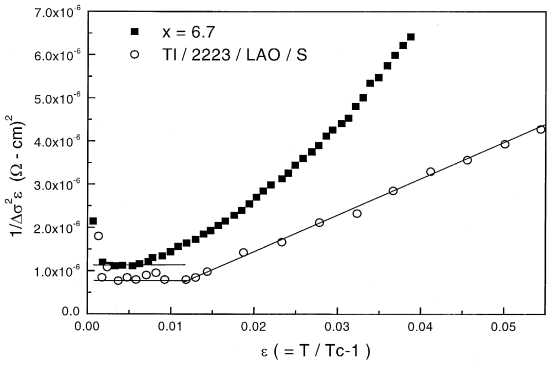

Fig. 5. $1/[\Delta\sigma^2(T)\varepsilon]$ as function of ε for YBCO with $x = 6.7$ and that of a Tl-2223 film. The lines are drawn to guide the eye.

lowering temperatures. The crossover sequence is opposite to that found in YBCO with $x > 6.7$, thus is not explainable by the A–L theory. Nevertheless, this is exactly what one would expect from the Lawrence–Doniach (L–D) theory [22]. Where the dimensionality of the system is governed mainly by the order parameter coupling (Josephson-like) between the adjacent conducting layers. Since the functional forms of $\Delta\sigma(T)$ are the same for each dimensionality in A–L and L–D theories, both d_{eff} and $\xi_c(0)$ can also be determined and are included in Table 1. For the Tl-2223 sample, the obtained d_{eff} and $\xi_c(0)$ are 4.4 and 0.2 Å, respectively. This indicates that Tl-2223 is a highly anisotropic material and the in-plane conductivity is confined within the triplicate CuO_2 units. For YBCO at $x = 6.7$, the calculated $\xi_c(0)$ is 0.6 Å, coinciding with the inferred extrapolated value of $\xi_c(T_{\text{cr}})$ (Fig. 4). Unfortunately, d_{eff}, in this case, is undetermined due to the absence of a well-defined T_{cr}. Finally, as listed in the last row of Table 1, the ratio between d_{eff} and $\xi_c(T_{\text{cr}})$ is the same in all cases, indicating a universal characteristic of the cuprate HTS. This suggests that there indeed exists a dimensional crossover in all HTS materials and within different regimes, one might need to use different theoretical analysis schemes to extract physically meaningful parameters.

4. Summary

In summary, we have presented a viable process to reproducibly manipulating the oxygen content of a

single YBCO film. By analyzing the $\Delta\sigma(T)$ data with a novel functional form, the effects of oxygen content on parameters such as d_{eff} and $\xi_c(0)$ are unambiguously determined. The results indicate that at $x \approx 6.7$, the prominent role of Cu–O chains in mediating the *c*-axis conduction in YBCO is completely suppressed and the system behaves more like the quasi-2D Tl-2223 material.

Acknowledgements

This work was supported by the National Science Council of Taiwan, R.O.C. through grant: NSC88-2112-M009-21.

References

[1] B. Oh *et al.*, Phys. Rev. B 37 (1988) 7861.
[2] S.J. Hagen, Z. Wang, N.P. Ong, Phys. Rev. B 38 (1988) 7137.
[3] T.A. Friedmann *et al.*, Phys. Rev. B 39 (1989) 4258.
[4] J.P. Rice, J. Giapintzakis, D.M. Ginsberg, J.M. Mochel, Phys. Rev. B 44 (1991) 10158.
[5] S.L. Cooper, K.E. Gray, in: D.M. Ginsberg (Ed.), Physical Properties of High Temperature Superconductors IV,1994, p. 61, and references therein.
[6] I. Bozovic, J.N. Eckstein, in: D.M. Ginsberg (Ed.), Physical Properties of High Temperature Superconductors IV,1996, p. 99, and references therein.
[7] R. Kleiner, F. Steinmeyer, G. Kunkel, P. Müller, Phys. Rev. Lett. 68 (1992) 2394.
[8] R. Kleiner, P. Müller, Phys. Rev. B 49 (1994) 1327.
[9] K.H. Wu *et al.*, Jpn. J. Appl. Phys. 37 (1998) 433.
[10] H.C. Lin *et al.*, Appl. Phys. Lett. 67 (1995) 2084.
[11] J.D. Joegensen *et al.*, Phys. Rev. B 41 (1990) 1863.
[12] M. Gurvitch, A.T. Fiory, Phys. Rev. Lett. 59 (1988) 1337.
[13] T. Ito, K. Takenaka, S. Uchida, Phys. Rev. Lett. 70 (1993) 3995.
[14] C.C. Homes *et al.*, Physica C 254 (1995) 265.
[15] L.D. Landau, E.M. Lifshitz, Statistical Physics, 3rd edn., Pergamon, 1980, Part 1, Chap. 12.
[16] M. Tinkham, Introduction to Superconductivity, 2nd edn., McGraw-Hill, New York, 1995, Chap. 8.
[17] L.G. Aslamazov, A.I. Larkin, Fiz. Tverd. Tela. (Leningrad) 10 (1968) 1104, [Sov. Phys. Solid State 10 (1968) 875].
[18] A. Frenkel, F. Gao, Y.F. Whitaker, C. Vher, S.Y. Hou, J.M. Philips, Phys. Rev. B 54 (1996) 1355.
[19] R.J. Cava *et al.*, Physica C 165 (1990) 419.
[20] R.E. Walstedt *et al.*, Phys. Rev. B 41 (1990) 9574.
[21] G. Uimin, Phys. Rev. B 50 (1994) 9531.
[22] W.E. Lawrence, S. Doniach, in: E. Kanda (Ed.), Proceedings of the 12th Low Temp. Phys., Kyoto, Japan, 1970, Keigaku, Tokyo, 1971, p. 361.